Applied Physics Letters

RESEARCH ARTICLE | OCTOBER 28 2025

Performance enhancement of GaN-based VCSELs by composition-graded structures

Special Collection: Frontiers in Nitride Semiconductors Research

Ya-Chao Wang ; Yu-Bing Xia ; Ai-Qin Tian ; Jian-Ping Liu ; Xiao-Bing Geng; Lei-Ying Ying ; Yang Mei ; Bao-Ping Zhang

Appl. Phys. Lett. 127, 173305 (2025)
https://doi.org/10.1063/5.0294456

Applied Physics Letters ARTICLE pubs.aip.org/aip/apl

Performance enhancement of GaN-based VCSELs by composition-graded structures

Cite as: Appl. Phys. Lett. **127**, 173305 (2025); doi: 10.1063/5.0294456
Submitted: 4 August 2025 · Accepted: 11 October 2025 ·
Published Online: 28 October 2025

Ya-Chao Wang,[1] Yu-Bing Xia,[1] Ai-Qin Tian,[2] Jian-Ping Liu,[2] Xiao-Bing Geng,[1,3] Lei-Ying Ying,[1] Yang Mei,[1,a)] and Bao-Ping Zhang[1,3,a)]

AFFILIATIONS

[1]Department of Microelectronics and Integrated Circuits, Xiamen University, Xiamen 361005, China
[2]Suzhou Institute of Nano-Tech and Nano-Bionics, Chinese Academy of Sciences, Suzhou 215123, China
[3]Institute of Nanoscience and Applications (INA) & College of Semiconductors, Southern University of Science and Technology (SUSTech), Shenzhen 518055, China

Note: This paper is part of the Special Topic on Frontiers in Nitride Semiconductors Research.
[a)]**Authors to whom correspondence should be addressed:** meiyang@xmu.edu.cn and bzhang@xmu.edu.cn

ABSTRACT

The carrier-injection efficiency and confinement within the active region play a crucial role in determining the threshold and slope efficiency of GaN-based vertical-cavity surface-emitting lasers (VCSELs). In this study, two types of composition-graded epitaxial structures were proposed: a composition-graded last quantum barrier (LQB) and a composition-graded electron blocking layer (EBL). GaN-based optically pumped VCSELs incorporating these structures exhibit significant improvements over conventional composition-uniform designs, with threshold reductions of 71.1% and 53.2%, respectively. Band structure analysis reveals that these performance improvements are attributed to enhanced electron injection efficiency and improved hole confinement within the active region as well. Furthermore, pulsed lasing operation in electrically injected VCSELs was demonstrated by employing the composition-graded LQB structure. This study systematically validated the effectiveness of the composition-graded LQB and EBL structures in improving GaN-based VCSEL performance from experimental perspectives. These findings provide valuable insights for the development of GaN-based VCSELs.

GaN-based vertical-cavity surface-emitting lasers (VCSELs) have attracted considerable attention owing to their unique advantages, including compact size, low threshold current, single longitudinal mode operation, and ease of integration into two-dimensional arrays.[1–3] In addition, GaN-based VCSELs exhibit significant application potential in solid-state lighting, displays, data communications, and high-density optical storage.[4–7] The output characteristics of GaN-based VCSELs, including lasing threshold, output power, and slope efficiency, are highly dependent on carrier-injection efficiency and confinement within the active region.[8–11] To address these challenges, various approaches have been proposed: Han simulated that introducing a p-AlGaN layer between the electron blocking layer (EBL) and p-GaN could enhance carrier-injection efficiency, thereby improving VCSEL performance.[12] However, from a growth perspective, this approach may not be feasible. Because AlGaN requires higher growth temperatures, the additional p-AlGaN layer could degrade the crystal quality of the active region. Wang proposed, based on simulations, that introducing an undoped GaN (u-GaN) layer between n-GaN and the first quantum well (QW) could enhance hole confinement in the active region but would simultaneously hinder electron injection.[13] They further suggested[14] increasing the p-type doping concentration in the EBL to improve hole-injection efficiency. While this strategy appears feasible in simulations, the growth of highly doped p-AlGaN remains a major challenge in epitaxial growth. We also proposed a composition-graded last quantum barrier (LQB) structure[15] located between the QW and the EBL and an N-polarity epitaxial structure[16] to enhance carrier injection and confinement in the active region, as predicted by simulations. However, N-polar epitaxy currently remains inferior to Ga-polar epitaxy. Additionally, An demonstrated that replacing a single AlGaN EBL with a five-pair AlGaN/GaN multi-quantum barrier electron blocking layer (MQB-EBL) effectively reduces carrier leakage from the active region.[17] This approach is also faced with challenges for epitaxial growth. Although these studies have shown promising simulation results, none has been experimentally validated to support their conclusions. The only experimentally verified approach is the composition-graded EBL structure reported by

Lin, which enhances carrier concentration in the active region and thereby improves VCSEL performance.[18] This study references this structure with some modifications.

As demonstrated in our previous studies,[15] composition-graded structures can modulate band bending by altering the distribution of polarization charges, thereby enhancing carrier injection and confinement, which ultimately improves device performance. In this study, experimental validation was carried out based on our previously simulated works. Two types of composition-graded epitaxial structures were designed and grown: one featuring an indium (In) composition-graded LQB, in which the In composition increases along the growth direction. The other featuring an aluminum (Al) composition-graded EBL, in which the Al composition decreases along the growth direction. For comparison, a conventional epitaxial structure was grown and used as a control sample. Optically pumped VCSEL devices were subsequently fabricated based on these three epitaxial structures. Experimental results demonstrated that both the composition-graded LQB and composition-graded EBL structures can improve VCSEL performance significantly, reducing the lasing threshold by 71.1% and 53.2%, respectively. Compared to the EBL design proposed by Lin, which features a gradually increasing Al composition,[18] our design—with a graded EBL of decreasing Al composition—exhibits a more pronounced reduction in the lasing threshold. The difference may arise from variations in polarization charge distribution and band tilting induced by the distinct Al composition profiles. Band structure analysis which was conducted using the PICS3D software reveals that these performance enhancements are primarily attributed to improved carrier-injection efficiency and confinement in the active region enabled by the composition-graded LQB and EBL structures. Furthermore, electrically injected VCSELs employing the composition-graded LQB structure were fabricated, achieving pulsed lasing at a near-green wavelength of 483 nm.

Samples were grown on sapphire substrates by using metal-organic chemical vapor deposition (MOCVD), with both the quantum wells (QWs) and quantum barriers (QBs) grown at a fixed temperature of 710 °C. InGaN/GaN multi-quantum wells (MQWs) were grown with a V/III ratio of 26 000 and an In concentration of 30%. The n-type GaN is with a Si doping concentration of $3 \times 10^{18}\,\mathrm{cm}^{-3}$, while the p-type GaN is with a Mg doping concentration of $1 \times 10^{19}\,\mathrm{cm}^{-3}$. The deposited pressure for InGaN QW was set to 400 mbar. Detailed growth parameters can be found in our previous work.[19] The three epitaxial structures designed in this study are illustrated in Fig. 1. The conventional structure (Structure A) consists of a 5 μm n-GaN layer, followed by an active region comprising four pairs of InGaN/GaN quantum wells (2 nm/5 nm), a 10 nm GaN LQB, a 15 nm AlGaN EBL, and an 88 nm p-GaN layer. The composition-graded EBL structure (Structure B) differs from Structure A solely in the EBL design, where the fixed 20% Al composition is replaced with a graded structure, decreasing from 20% to 0% along the growth direction. The composition-graded LQB structure (Structure C) differs from Structure A in the LQB design. The 10 nm GaN LQB is replaced with an 8 nm InGaN layer followed by a 2 nm GaN cap layer, and the In composition of the InGaN layer is linearly graded from 0% to 5% along the growth direction.

Figure 2(a) presents a cross-sectional transmission electron microscopy (TEM) image of the epitaxial wafer, where the Cr protection layer, p-GaN layer, EBL, LQB, MQWs, and n-GaN layer can be clearly distinguished from top to bottom. Figures 2(b) and 2(c) display the elemental distribution maps (EDS) of Al and In, respectively. One-dimensional Al and In elemental line-scan profiles were extracted

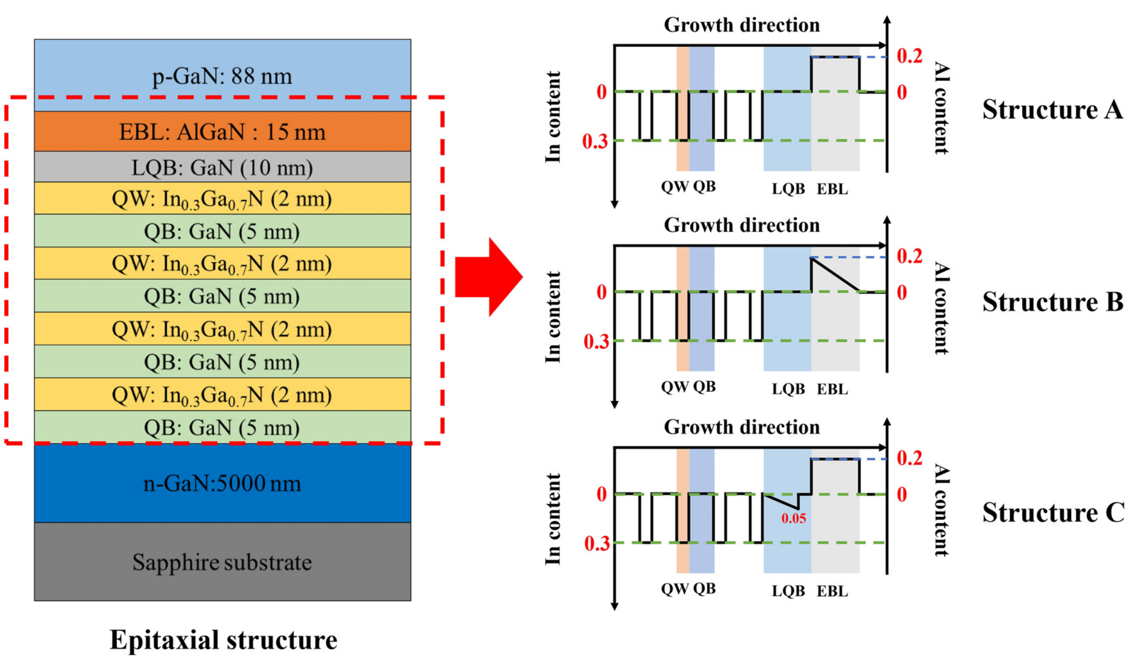

FIG. 1. Schematic diagrams of the epitaxial structures. Structure A: conventional structure; Structure B: an EBL design with a gradually decreasing Al composition along the growth direction; Structure C: an LQB design with a gradually increasing In composition along the growth direction.

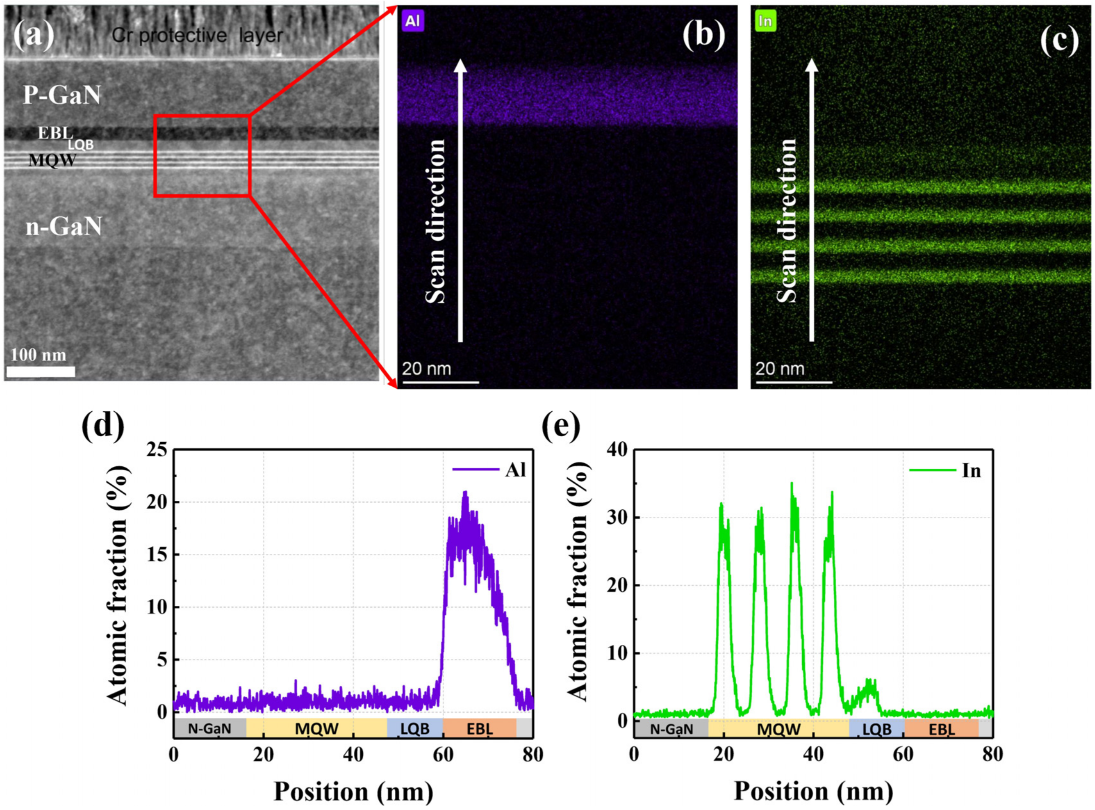

FIG. 2. (a) Cross-sectional TEM image of the epitaxial wafer (Structure B); (b) Al element distribution map in Structure B; (c) In element distribution map in Structure C; (d) Al atomic concentration profile extracted from Fig. 2(b); (e) In atomic concentration profile extracted from Fig. 2(c).

from Figs. 2(b) and 2(c), as shown in Figs. 2(d) and 2(e). The Al content in EBL decreases from 20% to 0% along the growth direction, while the In content in LQB increases from 0% to 5% along the growth direction. By using these epi-wafers, optically pumped VCSELs were fabricated, with similar processes in our previous work.[20] Briefly, 12.5 pairs of SiO_2/TiO_2 layers were first deposited on the epitaxial wafer to serve as the bottom distributed Bragg reflector (DBR). The sample was subsequently bonded onto a temporary substrate using UV-curable adhesive. The sapphire substrate was removed via laser liftoff. The exposed n-GaN layer was subjected to chemical mechanical polishing (CMP) to simultaneously reduce its thickness and surface roughness. Finally, a top DBR consisting of eight pairs of SiO_2/TiO_2 layers was deposited on the n-GaN side. The optical characteristics of the fabricated VCSELs were characterized at room temperature by using a photoluminescence (PL) measurement system. A 355 nm pulsed laser with a repetition rate of 15 kHz and a pulse width of 1 ns served as the excitation source. Both the excitation and emission signals were collected through the same objective lens, and the emission singles were directed to a charge-coupled device (CCD) and spectrometer for analysis.[21]

Figure 3(a) presents the PL spectra of the VCSEL fabricated using Structure A (Sample A) under varying pump densities. As the pump density increased from 8.6 to 24.4 mJ/cm^2, two lasing peaks emerge at approximately 475.1 and 478.0 nm. The inset shows near-field emission images of the device under three excitation power densities, with an excitation spot area of approximately 1555 μm^2. Two bright spots were observed in the images, corresponding to the two lasing peaks. The relationship between the peak intensity at 478.0 nm and the excitation power density is depicted in Fig. 3(b), revealing a threshold energy of approximately 21.8 mJ/cm^2. The lasing threshold was determined from the excitation power at which the PL intensity exhibited a sudden increase. To facilitate more intuitive comparisons among different samples and under varying excitation conditions for the same sample, we present the PL intensities in arbitrary units while maintaining fixed measurement conditions. Figure 3(c) illustrates the PL spectra of Sample A below and above threshold, clearly demonstrating the occurrence of stimulated emission.

Figure 4(a) presents the PL spectra of the VCSEL fabricated using Structure B (Sample B) under varying pump densities. As the pump density increased from 4.3 to 19.3 mJ/cm^2, four distinct lasing peaks sequentially emerged. At a pump density of 10.7 mJ/cm^2, a bright emission spot corresponding to the lasing peak at 473.7 nm was observed in the device. With further increasing of pump density, lasing was observed at additional locations within the device, each exhibiting a higher threshold. Moreover, different emission spots correspond to distinct lasing peaks. Figure 4(b) depicts the relationship between the peak intensity at 473.7 nm and the pump density, indicating a lasing threshold of approximately 10.2 mJ/cm^2. Figure 4(c) illustrates the PL spectra of Sample B below and above the lasing threshold.

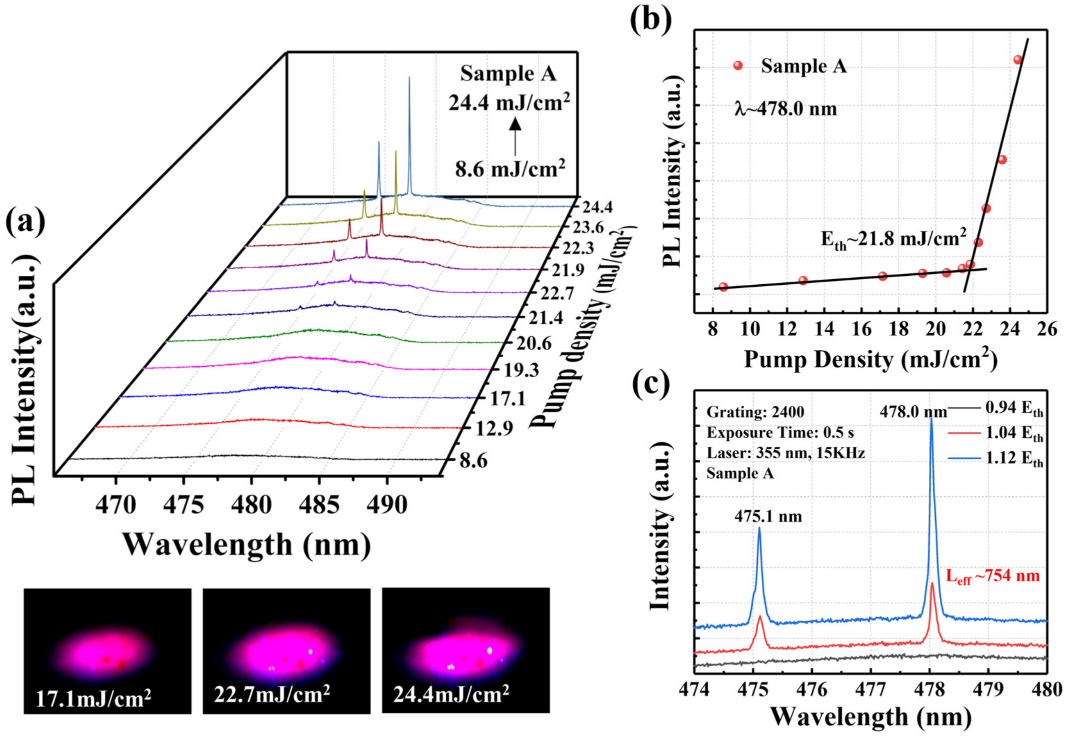

FIG. 3. Characteristics of VCSELs fabricated using Structure A: (a) PL spectra under varying pump densities, with insets showing near-field emission images; (b) relationship between PL intensity and pump density; (c) PL spectra below and above the lasing threshold.

Figure 5(a) presents the PL spectra of the VCSEL fabricated using Structure C (Sample C) under varying pump densities. As the pump density increased from 3.4 to 9.4 mJ/cm^2, lasing was observed at multiple locations within Sample C, accompanied by significantly higher emission brightness compared to Samples A and B. The appearance of multiple lasing spots in the three samples corresponds to spatially distinct lasing regions. This phenomenon arises from the inhomogeneity of the In composition, which causes variations in both threshold and emission wavelength at different locations. Consequently, the near-field emission manifests as discrete lasing spots rather than uniform lasing across the entire pumping area. These discrete lasing spots correspond to multiple lasing peaks observed in the spectrum. Figure 5(b) illustrates the relationship between the peak intensity at 478.4 nm and the pump density, indicating a lasing threshold of approximately 6.3 mJ/cm^2. Figure 5(c) shows the PL spectra of Sample C below and above the lasing threshold. The designed emission wavelengths of all three epi-wafer are in green spectral region of $\sim$500 nm. However, the lasing wavelength of the optical pumped VCSELs exhibited a blue shift to 470–480 nm. The higher photon energy and excitation density associated with the 355 nm laser induced a band-filling effect, shifting the gain spectrum toward shorter wavelengths.

Figure 6(a) shows the variation in PL intensity as a function of pump density for Samples A, B, and C. Sample A exhibited the highest lasing threshold and the lowest PL intensity. In comparison, the lasing thresholds of Samples B and C were reduced by 53.2% and 71.1%, respectively. In this study, the absolute output power of the optically pumped VCSELs was difficult to be accurately measured, and only the relative changes in slope efficiency are reported. While the slope efficiency of Sample A was normalized to 1, those of Sample B and Sample C turned out to be 1.13 and 41.59, respectively. These results are further analyzed in the following section through band structure. Figure 6(b) shows the repeatability test results of the three samples. Six positions are selected on each sample for measurement, and the results demonstrated good consistency. Sample A has the maximum threshold, followed by Sample B, and the minimum for Sample C.

The band structure of the samples is determined not only by the structural parameters but also by the electric field on both sides of the active region. This electric field is affected by the built-in electric field of the material, the external electric field, and the photovoltaic effect. The built-in electric field is determined by material properties, while the external electric field is zero under no-bias conditions, and the photovoltaic field arises under optical pumping. Figure 7(a) shows the equilibrium band diagram of the p–n junction under dark condition. When the p–n junction is illuminated with photons possessing energy greater than the bandgap, photogenerated carriers are separated by the built-in electric field: electrons in the p-type region are swept into the n-type region, and holes in the n-type region migrate into the p-type region. This carrier separation increases the potential on the p-side and decreases it on the n-side, thereby generating a photo-induced electromotive force across the junction, as illustrated in Fig. 7(b). This effect is equivalent to applying a forward bias voltage V across the p–n junction, corresponding to the open-circuit voltage V_{OC} in a photovoltaic device. The V_{OC} can be calculated as follows:[22]

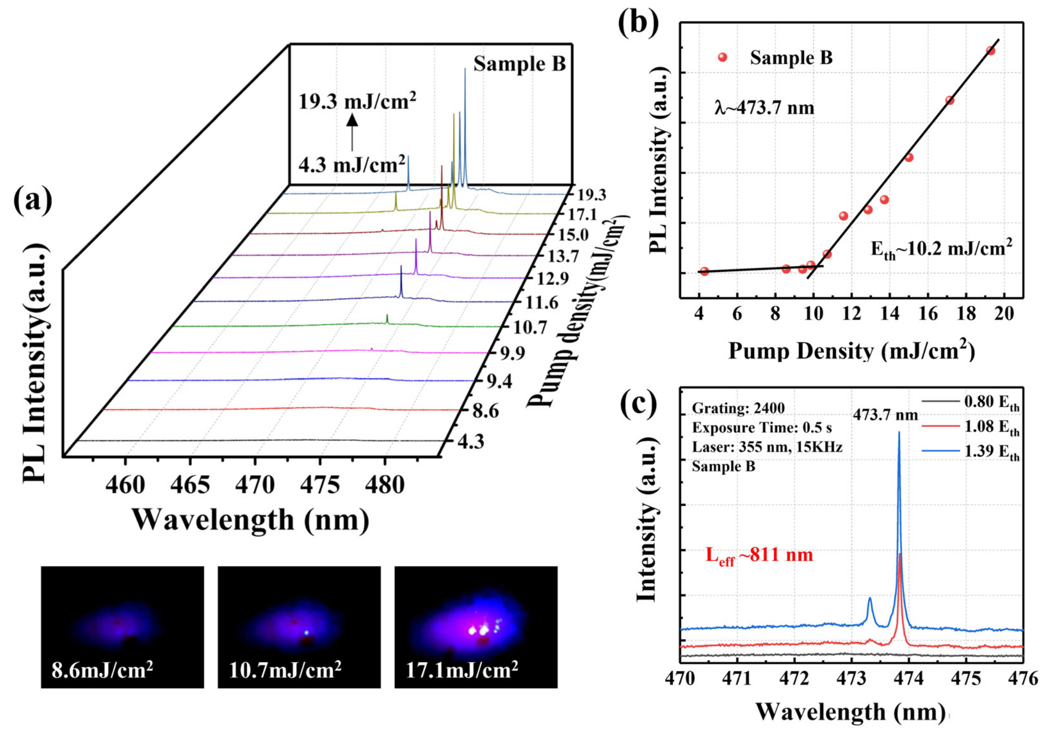

FIG. 4. Characteristics of VCSELs fabricated using Structure B: (a) PL spectra under varying pump densities, with insets showing near-field emission images; (b) relationship between PL intensity and pump density; (c) PL spectra below and above the lasing threshold.

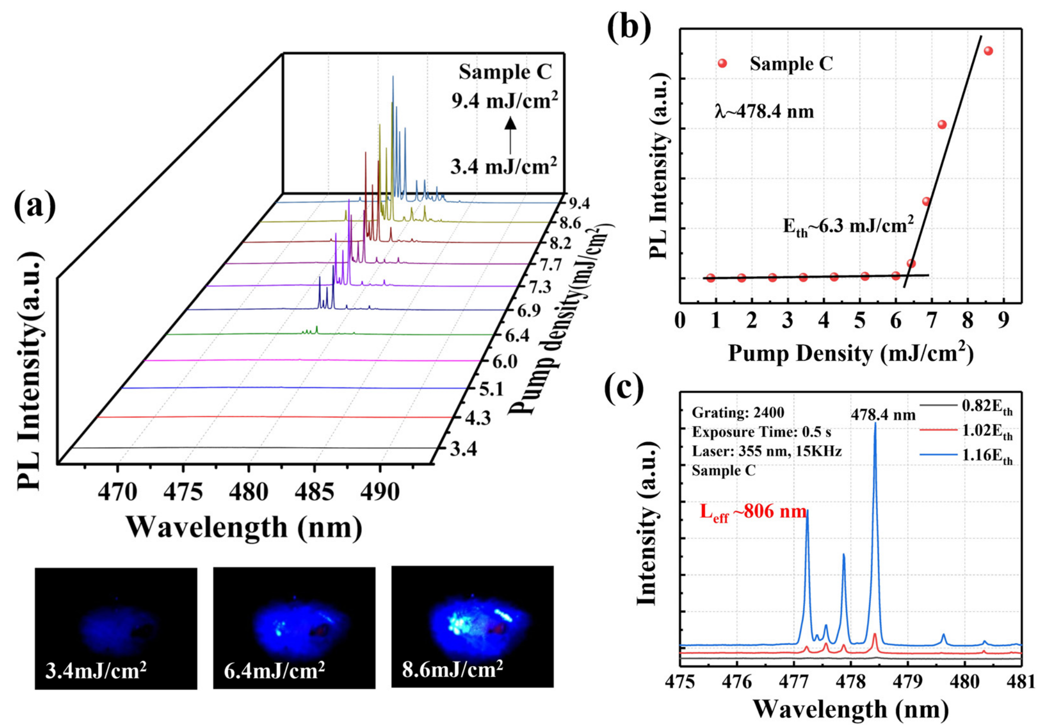

FIG. 5. Characteristics of VCSELs fabricated using Structure C: (a) PL spectra under varying pump densities, with insets showing near-field emission images; (b) relationship between PL intensity and pump density; (c) PL spectra below and above the lasing threshold.

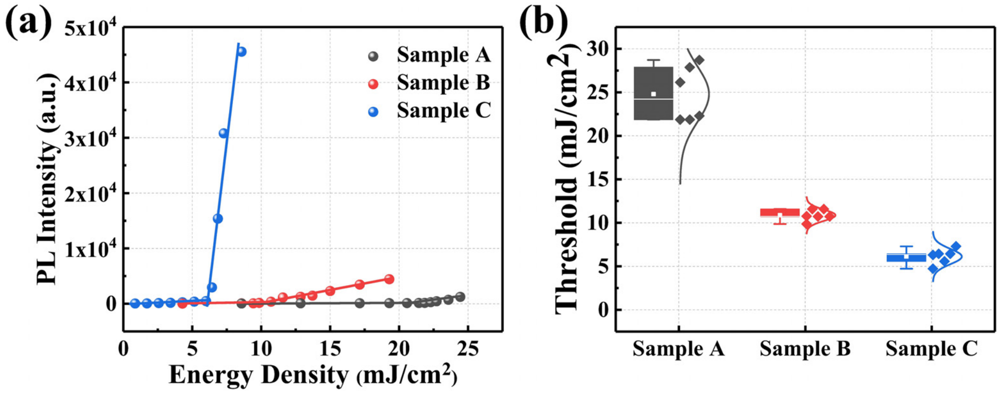

FIG. 6. (a) Comparison of PL intensity vs pump density for VCSELs fabricated using Structures A, B, and C; (b) repeatability test for the three samples.

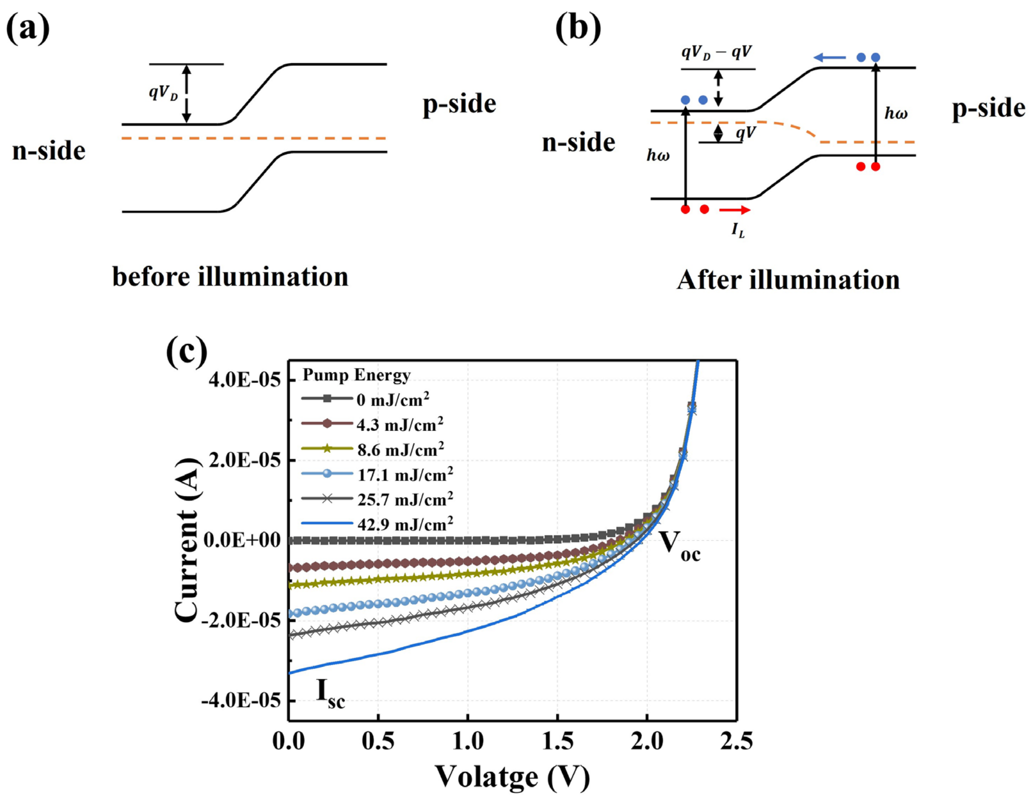

FIG. 7. (a) Energy band diagram of the p–n junction under dark conditions; (b) energy band diagram under optical pumping; (c) I–V characteristics of optically pumped VCSEL under varying excitation intensities.

$$V_{OC} = \frac{k_o T}{q} ln\left(\frac{I_L}{I_S} + 1\right), \quad (1)$$

where k_o is the Boltzmann constant, q is the elementary charge, and T is the temperature in K. I_L is the photo-induced current; I_S is the reverse saturation current. This indicates that during the operation of an optically pumped VCSEL, an internal forward bias voltage is present, which influences carrier transport. To determine the magnitude of this forward voltage, electrodes were fabricated on the optically pumped VCSELs and connected to a source meter to measure the current–voltage (I–V) characteristics under varying pump densities. The results are presented in Fig. 7(c). Based on I–V measurements and the relations derived from formula (1), V_{OC} corresponds to the open-circuit voltage (i.e., I_L=0), which reflects the photovoltage under

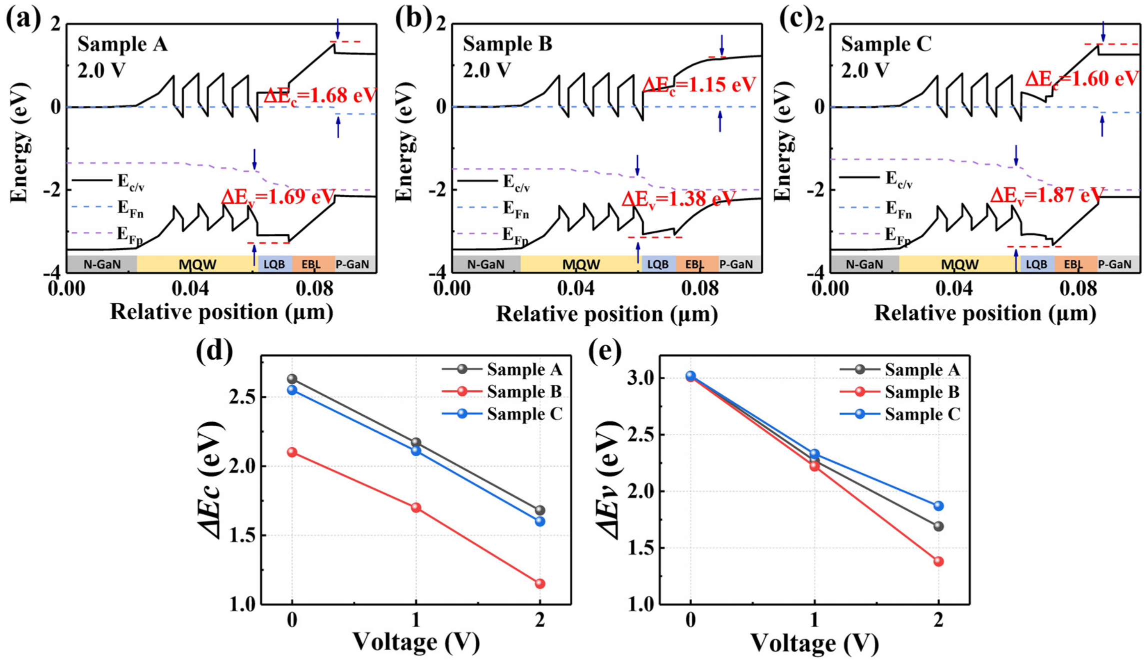

FIG. 8. Energy band diagram at a forward bias of 2 V: (a) Sample A; (b) Sample B; (c) Sample C; (d) electron injection barrier as a function of applied bias voltage for three samples; (e) hole blocking barrier as a function of applied bias voltage for three samples.

optical pumping. The V_{OC} increased with pump density and eventually saturated at approximately 2 V. Based on these measurements, band structure simulations for the three samples were performed using PICS3D software under forward bias voltages up to 2 V.

Figures 8(a)–8(c) represent the energy band diagrams of Samples A, B, and C under a forward bias of 2 V, respectively. The conduction band offsets are 690 meV for $In_{0.3}GaN$/GaN, 135 meV for $In_{0.05}GaN$/GaN, and 215 meV for $Al_{0.2}GaN$/GaN. Overall, the electron energy on the n-side is lower than on the p-side, causing photogenerated electrons to be injected from the p-side into the n-side, while photogenerated holes migrate in the opposite direction. Accordingly, the energy barrier between the EBL and p-GaN corresponds to the electron injection barrier (ΔEc), while the energy barrier between the last quantum well and p-GaN represents the hole blocking barrier (ΔEv). For Sample A, ΔEc is 1.68 eV and ΔEv is 1.69 eV; for Sample B, ΔEc is 1.15 eV and ΔEv is 1.38 eV; for Sample C, ΔEc is 1.60 eV and ΔEv is 1.87 eV. Figures 8(d) and 8(e) summarize the variations of ΔEc and ΔEv for Samples A, B, and C under forward biases ranging from 0 to 2 V, respectively. Regarding electron injection barriers, Sample B exhibits the lowest ΔEc (optimal injection), followed by Sample C. In terms of hole blocking barriers, Sample C exhibits the highest ΔEv (strongest confinement), followed by Sample A. Considering both electron injection and hole confinement, Sample C demonstrates simultaneous improvements in both aspects compared to Sample A. This simultaneous enhancement of electron injection and hole blocking capabilities leads to a 71.1% reduction in threshold energy for Sample C relative to Sample A, along with an improvement in slope efficiency and PL intensity. Although Sample B is featured with a reduced electron injection barrier, it exhibits the minimum hole blocking barrier, indicating a weak confinement to the hole. For GaN-based light emitting devices, the hole concentration and distribution inside the active region usually plays a more important role to the emission efficiency due to the lower mobility and amount when compared to that of electrons.[23,24] Therefore, it is reasonable that hole confinement plays a more decisive role than electron injection efficiency in determining PL performance in this study. The reduced hole confinement capability partially offsets the performance improvement achieved through enhanced electron injection efficiency, resulting in Sample B exhibiting a higher threshold current and lower slope efficiency compared to Sample C. On the other hand, the gradually decreasing Al composition in the EBL reduced the lattice mismatch with GaN,[25–27] which may be another reason for the improved performance of Sample B compared to Sample A. Therefore, the optically pumped VCSEL based on Sample C exhibits superior performance, indicating that the composition-graded LQB structure provides the most substantial improvement for GaN-based VCSELs.

Electrically injected devices were fabricated based on the composition-graded LQB structure. The schematic of the device structure is presented in Fig. 9(c). From top to bottom, the structure comprises of 8.5 pairs of SiO_2/TiO_2 layers serving as the top DBR, a 200 nm thick Cr/Au layer as the p-electrode, a 20 nm indium tin oxide (ITO) layer as the current spreading layer, with a current confinement aperture of 6 μm in diameter, achieved via boron ion (B^+) implantation. The sheet resistance of the ITO film was measured to be 43 Ω, and the absorption coefficient (α_{ITO}) was theoretically evaluated as 23 cm^{-1} in accordance with our previous work.[28] The detailed structure of the p-GaN, EBL, MQWs, and n-GaN layers is identical to those shown in Fig. 1. At the bottom, 12 pairs of SiO_2/TiO_2 layers form the bottom DBR, followed by a 100 μm thick electroplated copper layer, which serves as both the n-electrode and mechanical support substrate.

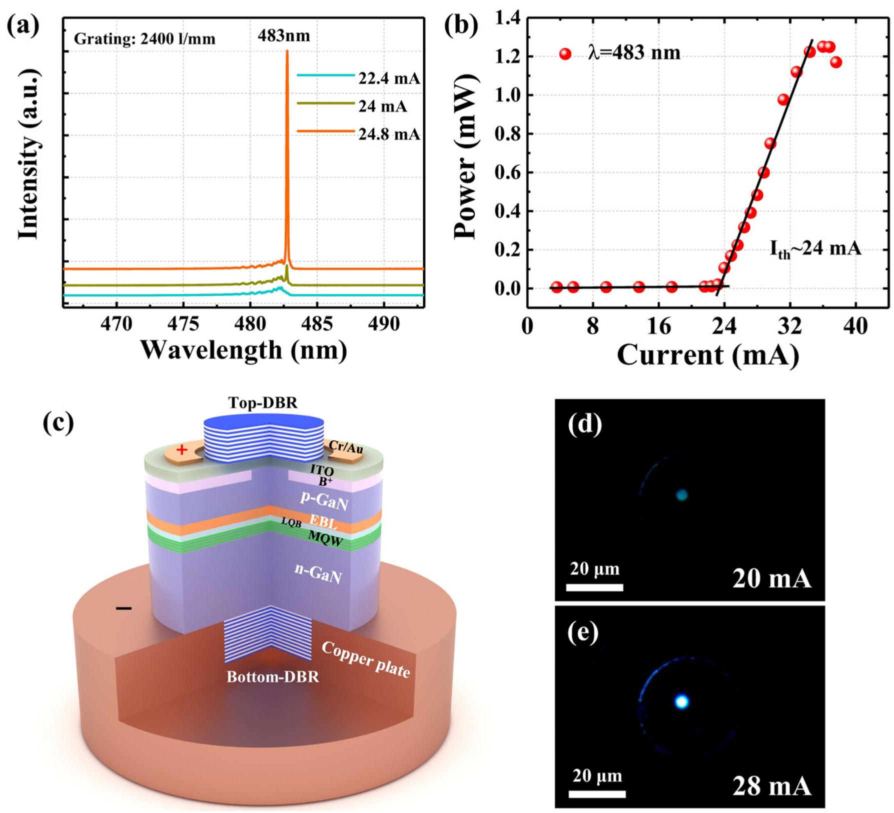

FIG. 9. Characteristics of the electrically injected VCSEL based on the composition-graded LQB structure: (a) EL spectra under different injection currents; (b) output power as a function of injection current, indicating lasing threshold; (c) schematic diagram of the GaN-based VCSEL structure; (d) and (e) are the near-field emission images of the device at 20 and 28 mA injection currents, respectively.

Figure 9(a) presents the electroluminescence (EL) spectra under different injection currents, obtained by using a pulsed current source with a pulse width of 100 ns and a duty cycle of 0.01%. The pulse width employed in this study is consistent with values reported in the literature,[29–31] whereas the reduced duty cycle was adopted to mitigate device heating during operation. As the injection current increased, the emission peak at 483 nm achieved lasing. Figure 9(b) shows the relationship between power and injection current, revealing a threshold current of approximately 24 mA and a maximum transient output power over 1.25 mW. Near-field emission patterns of the device were also captured, as shown in Figures 9(d) and 9(e), under injection currents of 20 and 28 mA, respectively. The device emission was confined to the center of the current aperture, demonstrating effective current confinement achieved through B^+ ion implantation. At 28 mA, clear lasing spots are observed within the aperture region.

In summary, three types of GaN-based VCSEL epitaxial wafers with distinct EBL or LQB structure were designed, grown, and used to fabricate GaN-based VCSELs. Experimental results demonstrate that both the Al composition-graded EBL and In composition-graded LQB structures can effectively reduce the lasing threshold and enhance the slope efficiency of the VCSELs, compared with the VCSEL with conventional EBL and LQB structure. Among these, the In composition-graded LQB structure exhibits superior performance, achieving a 71.1% reduction in threshold compared to the conventional structure, followed by the Al composition-graded EBL structure with a 53.2% reduction. Band structure simulations conducted using PICS3D reveal that these performance improvements originate from enhanced carrier-injection efficiency and hole confinement within the active region, enabled by the optimized LQB and EBL designs. Furthermore, an electrically injected VCSEL incorporating the composition-graded LQB structure was fabricated, demonstrating pulsed lasing operation. These results provide useful information for the development of high-performance GaN-based VCSELs.

This work was supported by the Shenzhen Science and Technology Program, (ZDSYS20220527171201003), the Natural Science Foundation of Guangdong Province (2025A1515011349), the National Natural Science Foundation of China (62474150, U21A20493, and 62234011), the National Key Research and Development Program of China (2024YFB3613100), and the Natural Science Foundation of Fujian Province (2023J05020).

The authors also thank Tao Yang, Lilong Ma, and Chenglong Chen for providing experimental support.

AUTHOR DECLARATIONS

Conflict of Interest

The authors have no conflicts to disclose.

Author Contributions

Ya-Chao Wang: Conceptualization (equal); Data curation (equal); Formal analysis (equal); Methodology (equal); Software (equal); Writing – original draft (equal); Writing – review & editing (equal).

Yu-Bing Xia: Data curation (equal); Investigation (equal); Project administration (equal). **Ai-Qin Tian:** Data curation (equal); Formal analysis (equal). **Jian-Ping Liu:** Data curation (equal); Formal analysis (equal). **Xiao-Bing Geng:** Conceptualization (equal). **Lei-Ying Ying:** Conceptualization (equal); Funding acquisition (equal). **Yang Mei:** Funding acquisition (equal); Resources (equal); Supervision (equal); Writing – review & editing (equal). **Bao-Ping Zhang:** Funding acquisition (equal); Writing – original draft (equal); Writing – review & editing (equal).

DATA AVAILABILITY

The data that support the findings of this study are available within the article.

REFERENCES

[1] H. Yu, Z. Zheng, Y. Mei, R. Xu, J. Liu, H. Yang, B. P. Zhang, T. Lu, and H. Kuo, Prog. Quantum Electron. **57**, 1–19 (2018).
[2] H. Xu, Y. Mei, R. B. Xu, L. Y. Ying, X. L. Su, J. P. Liu, and B. P. Zhang, Jpn. J. Appl. Phys., Part 1 **59**(SO), SO0803 (2020).
[3] C. Y. Huang, K. B. Hong, Z. T. Huang, W. H. Hsieh, W. H. Huang, and T. C. Lu, Micromachines **12**(6), 676 (2021).
[4] Å. Haglund, E. Hashemi, J. Bengtsson, J. Gustavsson, M. Stattin, M. Calciati, and M. Goano, Semicond. Lasers Laser Dyn. VII **9892**, 161 (2016).
[5] A. Liu, P. Wolf, J. A. Lott, and D. Bimberg, Photonics Res. **7**(2), 121 (2019).
[6] Y. Arakawa and T. Someya, in *IEEE Lasers and Electro-Optics Society 1999 Annual Meeting* (IEEE, 1999), Cat. No. 99CH37009, p. 389.
[7] G. Weng, Y. Mei, J. Liu, W. Hofmann, L. Ying, J. Zhang, Y. Bu, Z. Li, H. Yang, and B. P. Zhang, Opt. Express **24**(14), 15546 (2016).
[8] M. H. Kim, M. F. Schubert, Q. Dai, J. K. Kim, E. F. Schubert, J. Piprek, and Y. Park, Appl. Phys. Lett. **91**(18), 183507 (2007).
[9] J. Piprek, Phys. Status Solidi A **207**(10), 2217 (2010).
[10] J. Cho, E. F. Schubert, and J. K. Kim, Laser Photonics Rev. **7**(3), 408 (2013).
[11] V. Giovanni, S. Davide, M. Matteo, B. Francesco, G. Michele, M. Gaudenzio, and Z. Enrico, J. Appl. Phys. **114**(7), 071101 (2013).
[12] L. Han, Y. Gao, S. Hang, C. Chu, Y. Zhang, Q. Zheng, Q. Li, and Z. H. Zhang, Chin. Opt. Lett. **20**(3), 031402 (2022).
[13] Y. C. Wang, F. Liang, J. Yang, P. Chen, Z. S. Liu, C. Xia, and D. G. Zhao, Results Phys. **60**, 107690 (2024).
[14] Y. Wang, F. Liang, J. Yang, P. Chen, C. Xia, and D. Zhao, Opt. Express **32**(24), 42949 (2024).
[15] Y. C. Wang, T. Yang, L. Shi, Y. H. Chen, Y. Mei, and B. P. Zhang, Semicond. Sci. Technol. **38**(12), 125003 (2023).
[16] Y. C. Wang, Y. H. Chen, Z. M. Zheng, T. Yang, Y. Mei, L. Y. Ying, and B. P. Zhang, IEEE Photonics J. **16**(1), 1500606 (2024).
[17] B. An, Y. K. Wang, Y. C. Wang, Z. J. Zou, Y. Mei, H. Long, Z. W. Zheng, and B. P. Zhang, Photonics **11**(11), 1012 (2024).
[18] B. C. Lin, Y. A. Chang, K. J. Chen, C. H. Chiu, Z. Y. Li, Y. P. Lan, C. C. Lin, P. T. Lee, Y. K. Kuo, M. H. Shih, H. C. Kuo, T. C. Lu, and S. C. Wang, Laser Phys. Lett. **11**(8), 085002 (2014).
[19] A. Q. Tian, J. P. Liu, R. L. Zhou, L. Q. Zhang, S. Y. Huang, W. Zhou, M. Ikeda, S. M. Zhang, D. Y. Li, L. R. Jiang, H. Lin, and H. Yang, Appl. Phys. Express **12**(6), 064007 (2019).
[20] Y. Mei, T. R. Yang, W. Ou, Z. M. Zheng, H. Long, L. Y. Ying, and B. P. Zhang, Fundam. Res. **1**(6), 684 (2021).
[21] P. Gu, S. Yang, L. L. Ma, T. Yang, X. Hou, Y. Mei, L. Y. Ying, H. Long, and B. P. Zhang, Opt. Lett. **48**(15), 4117 (2023).
[22] S. M. Sze, Y. Li, and K. K. Ng, *Physics of Semiconductor Devices* (John Wiley & Sons, 2021).
[23] Z. H. Zhang, Z. G. Ju, W. Liu, S. T. Tan, Y. Ji, Z. Kyaw, X. L. Zhang, N. Hasanov, X. W. Sun, and H. V. Demir, Opt. Lett. **39**(8), 2483–2486 (2014).
[24] D. Y. Zhang, C. S. Chu, K. K. Tian, J. Q. Kou, W. G. Bi, Y. H. Zhang, and Z. H. Zhang, AIP Adv. **10**(6), 065032 (2020).
[25] Y. Y. Zhang and Y. A. Yin, Appl. Phys. Lett. **99**(22), 221103 (2011).
[26] J. H. Park, D. Y. Kim, S. Hwang, D. Meyaard, E. F. Schubert, Y. D. Han, J. W. Choi, J. Cho, and J. K. Kim, Appl. Phys. Lett. **103**(6), 061104 (2013).
[27] Y. Huang, Z. Y. Guo, M. Zhang, and D. Xiang, IEEE Access **9**, 65246 (2021).
[28] L. Y. Ying, X. L. Hu, W. J. Liu, J. Y. Zhang, B. P. Zhang, and H. C. Kuo, Superlattices Microstruct. **88**, 561 (2015).
[29] J. T. Leonard, E. C. Young, B. P. Yonkee, D. A. Cohen, T. Margalith, and S. P. DenBaars, Appl. Phys. Lett. **107**(9), 091105 (2015).
[30] J. T. Leonard, D. A. Cohen, B. P. Yonkee, R. M. Farrell, T. Margalith, S. Lee, S. P. DenBaars, J. S. Speck, and S. Nakamura, Appl. Phys. Lett. **107**(1), 011102 (2015).
[31] T. C. Chang, S. Y. Kuo, J. T. Lian, K. B. Hong, S. C. Wang, and T. C. Lu, Appl. Phys. Express **10**(11), 112101 (2017).